Modification of Alkanethiolate Self-Assembled Monolayers by Free Radical-Dominant Plasma

ARTICLE *in* THE JOURNAL OF PHYSICAL CHEMISTRY B · NOVEMBER 2001

Impact Factor: 3.3 · DOI: 10.1021/jp011119c

7 AUTHORS, INCLUDING:

Jiunn-Der Liao
National Cheng Kung University
99 PUBLICATIONS **910** CITATIONS

Modification of Alkanethiolate Self-Assembled Monolayers by Free Radical-Dominant Plasma

Jiunn-Der Liao,* Ming-Chen Wang, and Chih-Chiang Weng

Department of Biomedical Engineering, Chung Yuan Christian University, 22, Pu-Jen, Pu-Chung-Li, Chung-Li, Taoyuan 32023, Taiwan (ROC)

Ruth Klauser

Synchrotron Radiation Research Center, No. 1 R&D Road VI, Hsinchu Science-Based Industrial Park, Hsinchu 300, Taiwan (ROC)

Stefan Frey, Michael Zharnikov,* and Michael Grunze

Angewandte Physikalische Chemie, Universität Heidelberg, Im Neuenheimer Feld 253, D-69120 Heidelberg, Germany

Received: March 26, 2001; In Final Form: August 5, 2001

Synchrotron-based high-resolution photoelectron spectroscopy was applied to study the modification of the alkanethiol (AT) self-assembled monolayers on gold and silver substrates by nitrogen−oxygen downstream microwave plasma. Because of the low density and energy of the ionizing particles, the long-lived nitrogen and oxygen radicals provided the major impact of plasma treatment. The treatment resulted in massive damage and disordering of the initially well-ordered and chemically homogeneous AT films. The most pronounced processes are the complete (AT/Au) or partial (AT/Ag) oxidation of the pristine thiolate species, partial desorption of hydrogen and carbon-containing fragments with subsequent cross-linking within the residual hydrocarbon layer, and partial oxidation of this layer, and appearance of the nitrogen-containing entities. The plasma-treatment-induced changes in the alkyl matrix and at the S−substrate interface are only partly correlated. The rate and extent of the oxidation processes at this interface are noticeably larger for C18/Au than for C18/Ag, which suggests a stronger S−metal bond in the latter system. The results demonstrate that a smallest oxygen contamination should be avoided if one wants to perform a soft modification of thin organic layers or definite molecular entities attached to these layers through the exposure to plasma.

1. Introduction

During the last two decades, close-packed arrays of amphiphilic molecules, called self-assembled monolayers (SAMs), have attracted considerable interest from both the scientific and practical viewpoints.[1,2] Considering the practical aspect, these films, in which the headgroup of an adsorbate covalently bonds to a solid substrate, while the chainlike molecular tail sticks out from the substrate, provide a means to tailor surface properties, such as wetting, lubrication, adhesion, and corrosion. These properties can be controlled by both the selection of suitable molecules and the physical modification of the respective SAMs through their exposure to ions,[3] X-ray photons,[4−7] UV-light,[8−12] or electrons.[13−22] Depending on the SAM choice, such an exposure results in either partial or total damage of the pristine film,[7,22] its quasi-polymerization,[23] and chemical modification of the tail group attached to the molecular chain.[24,25] In particular, low-energy electron irradiation results in the transformation of the nitro tail group in 4-nitro-1,1′-biphenyl-4-thiol SAM on gold into amino group, which can be subsequently used for the attachment of proteins and cells to the modified SAMs.[25] Provided that the SAM modification is performed by a homogeneous irradiation through a mask or a focused electron/photon beam is scanned in a desired way over the sample surface, micro- and even nanostructuring of a SAM can be performed and the structured SAM can be used as a positive or negative resist within the "conventional" lithography approach or as a template in the chemical lithography framework.[26−36]

One of the perspective but nonsufficiently developed methods of physical modification of SAMs is plasma processing. Whereas this method is widely applied in microelectronics for chemical modification, etching, and patterning of organic surfaces and thin organic films, there are only a few examples for the plasma treatment of SAMs. In particular, Lercel et al.[33] used a low-pressure, high-density $Cl_2/BCl_3/CH_4$ electron cyclotron resonance plasma for the patterning of octadecylthiol SAMs on GaAs. Unger et al. succeeded in the partial oxygen functionalization of octadecyltrichlorilane films on an oxidizing silicon wafer using a low-pressure oxygen direct current plasma.[37]

A major reason for the rather restrained activities concerning the plasma treatment of SAMs is presumably a large complexity of the physical and chemical processes occurring during the interaction of plasma with these systems. Both the ionizing species such as ions, electrons, free radicals, and the UV-light generated by plasma affect a SAM film at the same time. Considering that the plasma composition and the energies of

* Corresponding authors: J.-D. Liao (E-mail: jdliao@mail.be.cycu.edu.tw) and M. Zharnikov (E-mail: Michael.Zharnikov@urz.uni-heidelberg.de).

10.1021/jp011119c CCC: $22.00
Published on Web 12/01/2001

plasma constituents depend on the type and mode of generation[38−41] and taking into account that every of these constituents interacts with a SAM in its specific way, one is confronted with a very complex situation. The problems can be, however, simplified if at least a partial characterization of plasma is performed and a well-established SAM system is taken.

In this study we applied nitrogen downstream microwave plasma to SAMs of alkanethiols (AT) on polycrystalline (111) Au and Ag substrates. The SAMs were placed into a plasma afterglow region separated by an extensive flowing pathway from the zone, where plasma excitation by the microwave field was performed. We expected that this positioning will enable to expose the SAMs predominantly to free radicals and minimize the effects producing by other plasma constituents, especially by electrons and ions.[39,40,42−44] Due to numerous collisions of these species with the walls of the pathway quartz tube during their transfer to afterglow region, they lose kinetic energy and become incapable of re-exciting neutrals or affecting a SAM to a noticeable extent. However, it was very likely that adsorbates on the walls of the pathway quartz tube, typically oxygen-containing substances, will be partially removed by plasma flow, recombined with nitrogen plasma as oxygen-containing nitrogen plasma, and projected to the surface of SAMs. Note that oxygen in different excited forms is chemically much more reactive, compared with similar states of nitrogen.[41,45]

The choice of AT SAMs as an object of the plasma treatment is related to the large popularity of these systems, which probably are the best studied SAMs by present and are often used as model SAM films.[2] The chainlike AT molecules are bonded to the substrate via their sulfur headgroup forming a c(4 × 2) modulated commensurate ($\sqrt{3} \times \sqrt{3}$) R30° lateral lattice on Au(111) surfaces and an incommensurate ($\sqrt{7} \times \sqrt{7}$) arrangement on the Ag(111) substrates.[1,46−49] The resulting larger packing density in AT/Ag is accompanied by a smaller inclination of the AT chains as compared to AT/Au. The average tilt angles of AT chains in AT/Ag and AT/Au are 10−12° and 27−33°.[1,2,46] Additionally, there are some indications for the different strengths of thiolate−substrate bonding for these two systems,[46,50] namely, for a stronger thiolate−substrate bond for AT/Ag as compared to AT/Au.[3,22,51]

Plasma treatment of AT SAMs should predominantly result in their damage.[33] In particular, the exposure of these films to electrons with the energy higher than ∼5−7 eV[17,21] causes the loss of the orientational and conformational order, partial dehydrogenation with C═C double bond formation, desorption of the layer fragments, reduction of the thiolate species, and the appearance of alkylsulfide species.[7,16,19,20,22] The UV photooxidation of the AT SAMs leads to the oxidation of the thiolate headgroup to sulfonate, disordering, and partial desorption of the molecular fragments.[9−11] The ion bombardment of the AT films induces the layer fragmentation, cleavage of C−S and S−substrate bonds, and the formation of C═C double bonds.[3] It is interesting to find out whether the effects provided by free radicals-dominant plasma differ from the above-mentioned phenomena and whether a "soft", nondestructive plasma treatment is possible to vary the chemical identity of the tail group for potential microelectronic and biomedical applications.[52,53] Another important aspect, which was the primary reason to study both AT/Au and AT/Ag, is a possible difference in the resistance toward the plasma treatment between these two systems. The analogous effects have been found for the photooxidation[10,11] and the ion- and electron-induced damage.[3,22]

In the following, we will give a brief description of the experimental procedure and setup with a special emphasis on the design of the plasma source and on the plasma characterization. Thereafter, the results are presented and preliminarily discussed in Section 3. An extended analysis of the data is given in Section 4. Finally, the results are summarized in Section 5.

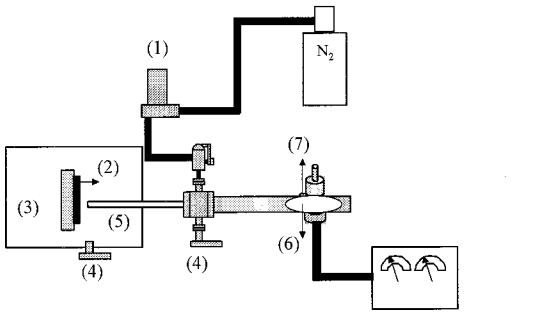

Figure 1. Schematic experimental setup of the plasma source attached to the preparation chamber.

2. Experimental Section

The substrates were prepared by evaporation of 100−300 nm of gold or silver on titanium-primed (5 nm) polished single-crystal Si(100) wafers (Silicon Sense). These films predominantly exhibit an (111) orientation as, e.g., concluded from the distinctive forward-scattering maxima in the angular distributions of the Au 4f and Ag 3d photoelectrons[54] and from the characteristic binding energy (BE) shift of the Au 4f surface component.[55] The SAMs were formed by immersion of the substrates in an ethanolic 1 mM solution of octadecanthiol [C18: $CH_3-(CH_2)_{11}-SH$] (Fluka Chemicals) for 24 h. After the immersion, the samples were carefully rinsed and cleaned with ethanol, and blown with dry and pure nitrogen. The contact angle of the C18 SAMs (measured by the sessile drop method) was found to be ∼108 ± 2°, as could be expected for the hydrophobic CH_3 surface.

Plasma treatment was performed in a special UHV preparation chamber attached to the analysis chamber (see below). The C18/Au and C18/Ag samples were fixed on the sample holder in front of the outlet of a quartz tube (inner diameter of 5 mm) leading to the plasma glow discharge region (see Figure 1). The distance between the sample surface and this region was about 170 mm and between the sample and nozzle head about 10 mm. The glow discharge microwave plasma was produced using a microwave (∼2.45 GHz) plasma generator (OPTHOS Instruments Inc.) with a power of 80 W. A flow rate of 500 sccm for N_2 gas (purity of 99.9999%) was maintained by keeping a pressure of ∼1 Torr in the plasma processing chamber. The pressure in the gas-discharged region was about 13 Torr.

The afterglow plasma in the vicinity of the sample, inside the preparation chamber, was characterized using the Langmuir probe (Figure 2) connected to an electrometer (Keithley, model 6514). This invasive, electrostatic probe utilizes 10 mm long tungsten wire of 0.25 mm in diameter as the probing tool. Using the $I-V$ curves provided by this device, plasma density (or ionization density) was calculated according to the equations

$$N_\infty \equiv N_{e\infty} = 4\frac{I_{se}}{eA_p\bar{v}_e} \quad (1)$$

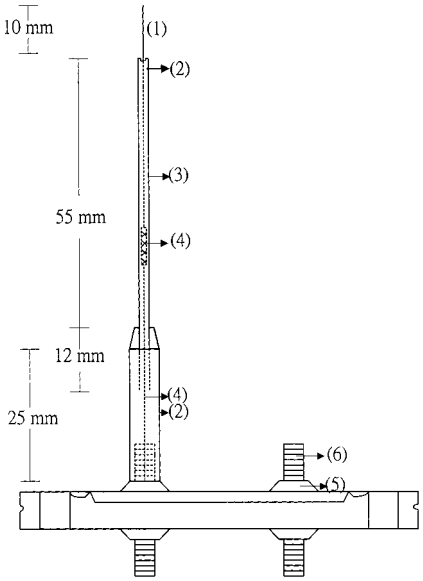

Figure 2. Layout of *Langmuir* probe. (1) Tungsten wire with a diameter of 0.25 mm and a length of 50 mm; (2) PTFE isolation; (3) quartz tube; (4) conductive Ag wire; (5) PTFE isolation; (6) Cu electrode.

$$N_\infty = \frac{\pi}{A_a}\left(\frac{Sm}{2e^3}\right)^{1/2} \tag{2}$$

where N_∞ and $N_{e\infty}$ are the plasma and electron densities, respectively, I_{se} is the current at saturation (e.g., calculated from the $I-V$ curve as shown in Figures 3a and 3b), A_p is the exposed surface area of the probe, A_a is the number of collected charged particles, $\bar{v}_e$ is the average speed of electrons, S is the electron flux, and m and e are the mass and the charge of electron. The electron temperature T_e was estimated on the basis of the derivate $I-V$ curves (as, for example, in Figure 3b), according to the equation

$$\ln\left(\frac{I_e}{I_{se}}\right) = \frac{e}{kT_e}(V - V_p) \tag{3}$$

where I_e is the electron current, k is Boltzmann's constant, V is the external bias voltage, and V_p is the plasma potential.

Expressions 1−3 are simplifications derived for the Langmuir probe within so-called Thin Sheath Theory (eqs 1 and 3) and Thick Sheath Theory (eq 2).[42,43] The following assumptions have been made: (1) the potential of the Langmuir probe was regarded as quasi-neutral without environmental interference before testing; (2) the numbers of ions and electrons are dynamically equal; (3) the mean free paths of ions and electrons are significantly larger than the length of the probe; (4) the temperature of electrons is much higher than that of ions or neutrals; (5) the diameter of the probe is much larger than the Debye wavelength of electron; (6) energy distribution of ions and electrons is described by the Maxwellian theory (see refs 39, 42, and 43 for details).

The C18/Au and C18/Ag samples were simultaneously exposed to the afterglow plasma for either 2 or 4 min. Note that although the plasma basically consisted of nitrogen-derived species, there was a portion of oxygen-derived species (presumably free radicals) originated from the walls of the preparation chamber and plasma-pathway tube.

The characterization of both the pristine and plasma-treated AT films was performed by high-resolution X-ray photoelectron spectroscopy (HRXPS). Measurements were carried out at the U5 undulator beamline of the Synchrotron Radiation Research Center in Hsinchu, Taiwan. For doing the HRXPS characterization the samples were directly transferred to the UHV analysis chamber attached to the preparation chamber and equipped with a CLAM-4 9-channeltron electron energy analyzer (VG Microtech). An excitation energy of 390 eV was utilized to measure the Au 4f, S 2p, and C 1s core level spectra, while the Ag 3d, N 1s, and O 1s spectra were acquired with a photon energy of 650 eV. The energy resolution was 0.2−0.3 eV. The energy scale was referenced to the pronounced Au $4f_{7/2}$ "bulk" peak (84.00 eV) of the C18/Au sample.[55] The energy calibration was performed for every sample and after every change of the photon energy to exclude effects related to the instability of the monochromator. Special care was taken to avoid X-ray radiation-induced damage during the spectra acquisition.[7]

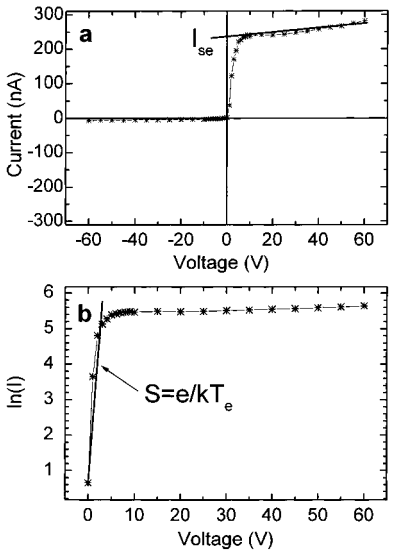

Figure 3. $I-V$ curve measured by Langmuir probe. The curve is fitted using Thin Sheath Theory. The $\ln(I)-V$ curve derived from the $I-V$ curve in (a) is shown in (b). The slope (S) of the $\ln(I)-V$ curve at low voltages is used to estimate the electron temperature of the plasma (T_e).

The spectra were fitted using Doniach-Sunjic peak profiles and Shirley background. To fit the S $2p_{3/2,1/2}$ doublet we used a pair of such peaks with the same fwhm, the standard[56] spin−orbit splitting of ∼1.2 eV (verified by the fit) and the branching ratio of 2:1 (S $2p_{3/2}$/S $2p_{1/2}$). The resulting accuracy of the BE/fwhm values given in this letter is ∼0.05 eV for both the S 2p and C 1s peaks.

The XPS peak intensities $I(x)$ were utilized to determine surface stoichiometric ratios of different film constituents a and b according to[57]

$$N(a)/N(b) = I(a)/I(b) \times (C_b/C_a) \tag{4}$$

where $I(a)$ and $I(b)$ are the measured peak intensities, and C_a(and C_b are the correction terms

$$C_x = \sigma_{Ekin}(x) \times T_{Ekin}(x) \times f(\lambda_{Ekin}) \tag{5}$$

where $\sigma(x)$ is the photoionization cross-section of the probed core-level, $T_{Ekin}(x)$ is the transmission of the spectrometer, and $f(\lambda_{Ekin})$ is a function describing the attenuation of the photoelectron signal at a given kinetic energy, this function depends on the electron mean free path λ_{Ekin}.

3. Results

3.1. Plasma Density and Plasma Species. The plasma characterization in the afterglow region was performed both

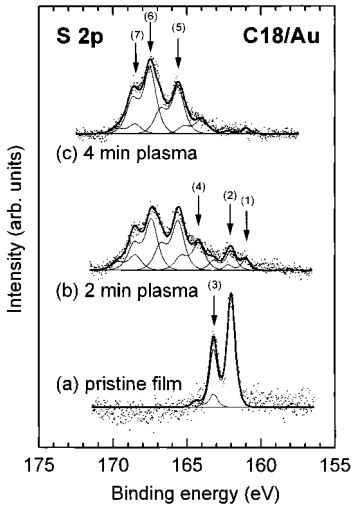

Figure 4. S 2p HRXPS spectra and peak assignments for C18/Au before (a) and after the plasma treatment for 2 min (b) and 4 min (c). Peak assignment: (1) 161.0 eV, atomic sulfur; (2) 162.02 eV, thiolate; (3) 163.2 eV, alkylsulfide; (4) 164.2 eV, cysteine; (5) 165.6 eV, SO; (6) 167.5 eV, SO_3; (7) 168.5 eV, SO_4.

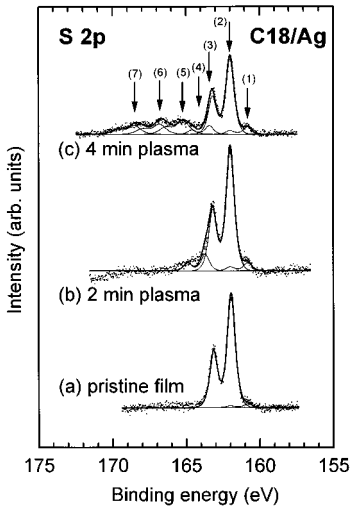

Figure 5. S 2p HRXPS spectra and peak assignments for C18/Ag before (a) and after the plasma treatment for 2 min (b) and 4 min (c). Peak assignment: (1) 160.9 eV, atomic sulfur; (2) 161.93 eV, thiolate; (3) 163.3 eV, alkylsulfide; (4) 164.0 eV, cysteine; (5) 165.5 eV, SO; (6) 166.7 eV, SO_2; (7) 168.5 eV, SO_4.

separately and during the plasma treatment of the AT films. Twenty successive measurements were carried out to get the desired statistical accuracy. The density of electrons (or ions) in the downstream afterglow nitrogen microwave plasma was estimated as $1.37 \pm 0.22 \times 10^6$ particles/cm^3 and the electron temperature was determined as ~5500 K. A typical $I-V$ curve provided by the Langmuir probe and the corresponding $\ln(I)-V$ curve are displayed in Figures 3a and 3b, respectively. The electron density (ionization density) was calculated by eq 1 on the basis of the $I-V$ value of the current at saturation (I_{se}) derived from the high voltage region of the $I-V$ curve. The electron temperature (T_e) was derived from the slope S of the $\ln(I)-V$ curve in the low voltage region using the simplifications of the Thin Sheath Theory (eq 3). A derived electron temperature of ~5500 K implies that the plasma in the afterglow region has low energy of ~0.5 eV and the derived density of electrons suggests a relatively low density of the ionizing particles. Note for comparison, that the plasma density of the antenna-coupling microwave (~2.54 GHz) plasma determined with the same Langmuir probe exceeds 10^{10} particles/cm^3, while this value for the radio frequency (~13.56 MHz) plasma with bias electrodes is estimated as more than 10^9 particles/cm^3.[40,41,44,58] Going back to the afterglow plasma of this study, we believe that its major components in the vicinity of the samples are the long-lived N*, N*$_2$, O*, and O*$_2$ free radicals, the portion of the nitrogen-derived radicals being significantly larger.

3.2. Pristine C18/Au and C18/Ag and Plasma-Induced Changes. The S 2p, C 1s, and O 1s HRXPS spectra of the pristine (a) and the plasma-treated (b,c) C18/Au samples are presented in Figures 4, 6, and 8, respectively. The corresponding spectra for C18/Ag are depicted in Figures 5, 7, and 9. The N 1s HRXPS spectra of the plasma-treated C18/Au and C18/Ag samples are shown in Figure 10.

For the pristine films no traces of oxygen and nitrogen were found. The S 2p spectra exhibit a single S 2p doublet with BEs (S $2p_{3/2}$) of 162.02 and 161.93 eV for C18/Au and C18/Ag, respectively. The observed doublet is commonly related to the thiolate species bonded to the gold surface.[7,46,55,59] Note that the BEs of this doublet correlate very well with the analogous values of 161.91 eV (C12/Au) and 161.84 eV (C12/Ag) obtained in recent HRXPS study by Heister et al.[55] Also the fwhms of the S $2p_{3/2}$ and S $2p_{1/2}$ peaks in Figures 4 and 5 (0.67 and 0.69 eV, respectively) agree excellently with the corresponding values of 0.54 and 0.58 eV of ref 55 considering a lower energy resolution (0.25 eV vs 0.1 eV in ref 55) of the present study. The C 1s spectra of the pristine AT films in Figures 6a and 7a exhibit a single emission peak at 284.9 eV for C18/Au and 285.3 eV for C18/Ag with identical fwhms of ~0.9 eV in good agreement with previous XPS[22] and HRXPS[55] studies.

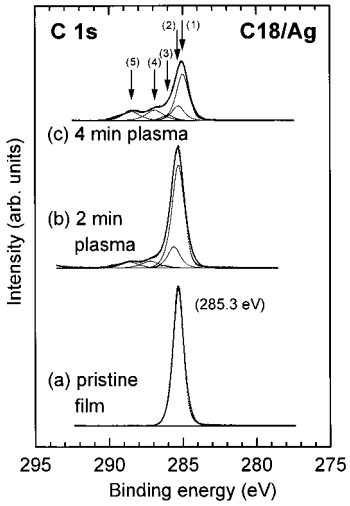

Figure 6. C 1s HRXPS spectra and peak assignments for C18/Au before (a) and after the plasma treatment for 2 min (b) and 4 min (c). Peak assignment: (1) 284.9 eV, C−C; (2) 285.3 eV, C*−C−O; (3) 286.0 eV, C−N; (4) 286.8 eV, C−O; (5) 288.3 eV, C═O.

The plasma treatment results in noticeable changes in the S 2p and C 1s HRXPS spectra of both C18/Au and C18/Ag and in the appearance of the characteristic traces of oxygen and nitrogen in the O 1s and N 1s spectra. To follow these changes the respective spectra in Figures 4−10 are decomposed to the individual spectral components related to the definite chemical moieties in the plasma-treated films. The assignment of these components has been performed in according with refs 7, 10, 22, 56, 60, and 61. The relative intensities of the derived peaks are presented in Tables 1 and 2. These values were obtained on the basis of eqs 4 and 5.

The C 1s spectra for both C18/Au and C18/Ag change in a similar way in the course of the plasma exposure (see Figures

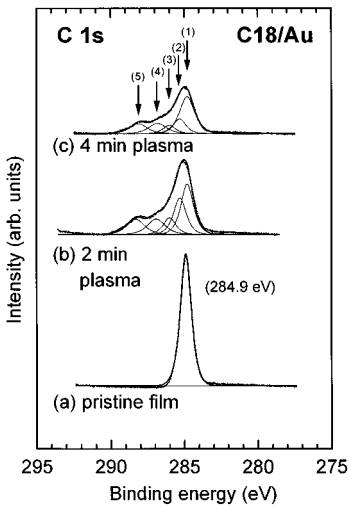

Figure 7. C 1s HRXPS spectra and peak assignments for C18/Ag before (a) and after the plasma treatment for 2 min (b) and 4 min (c). Peak assignment: (1) 284.9 eV, C═C; (2) 285.3 eV, C−C; (3) 286.0 eV, C−N; (4) 286.9 eV, C−O; (5) 288.4 eV, C═O.

TABLE 1: Quantitative Evaluation of C 1s Peak Intensities for the Pristine and Plasma-Treated C18/Au and C18/Ag (see Figures 6 and 7)[a]

	Au substrate		Ag substrate	
intensity ratio	N_{C1s}/N_{Au4f}	$N_{C1s(main)}/N_{Au4f}$	N_{C1s}/N_{Ag3d}	$N_{C1s(main)}/N_{Ag3d}$
pristine film	1.00	1.00	1.00	1.00
2 min plasma	0.95	0.59	0.91	0.88
4 min plasma	0.81	0.53	0.80	0.48

[a] N_{C1s} and $N_{C1s(main)}$ are the entire C 1s intensity and the intensity of the main C 1s emission at 285.1−284.8 eV, respectively (the BEs of the C 1s peak are different for C18/Au and C18/Ag; there is a downward shift of these values upon the plasma treatment, see text). The intensity ratios of the pristine films have been taken as 1.00.

TABLE 2: Quantitative Evaluation of the O 1s and S 2p Peak Intensities for the Pristine and Plasma-Treated C18/Au and C18/Ag (see Figures 4, 5, 8 and 9)[a]

	Au substrate		Ag substrate	
intensity ratio	N_{O1s}/N_{Au4f}	N_{S2p}/N_{Au4f}	N_{O1s}/N_{Ag3d}	$N_{S2p}/N_{Ag\ 3d}$
pristine film	0.0	0.018	0.0	0.035
2 min plasma	0.021	0.031	0.013	0.032
4 min plasma	0.015	0.028	0.023	0.018

[a] N_{S2p} and N_{O1s} are the entire S 2p and O 1s intensity, respectively. All ratios for Au and Ag substrates are normalized to the N_{C1s}/N_{Au4f} and N_{C1s}/N_{Ag3d}, respectively (see Table 1).

6 and 7). The intensity of the C 1s peak related to the intact alkyl chains in the well-ordered SAMs decreases, a downward shift and broadening of this peak occur, and a variety of new features on the higher BE side of the main emission evolve. The majority of these features could be assigned to different oxygen-containing moieties and only the peak at ∼286.0 eV was ascribed to the nitrogen-containing C−N group (see also the N 1s spectra in Figure 10). The occurrence of the oxygen-containing species in the plasma-processed C18 films is supported by the O 1s spectra in Figures 8 and 9, which are qualitatively similar (but quantitatively different) for C18/Au and C18/Ag. As to the nitrogen-containing compounds originated from the N* and N_2* free radicals, their amount increases at first and then begins to decrease in the course of the plasma exposure (Figures 10a and 10b), which (at least for C18/Au) correlates with the development of the C−N and O−N peaks in Figures 6 and 8, respectively.

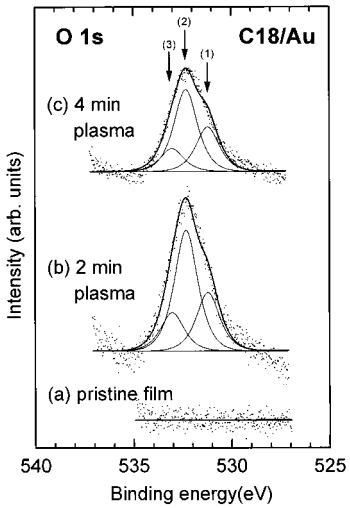

Figure 8. O 1s HRXPS spectra and peak assignments for C18/Au before (a) and after the plasma treatment for 2 min (b) and 4 min (c). Peak assignment: (1) 531.2 eV, C−O and SO; (2) 532.3 eV, SO_n ($n > 1$); (3) 533.0 eV, N−O.

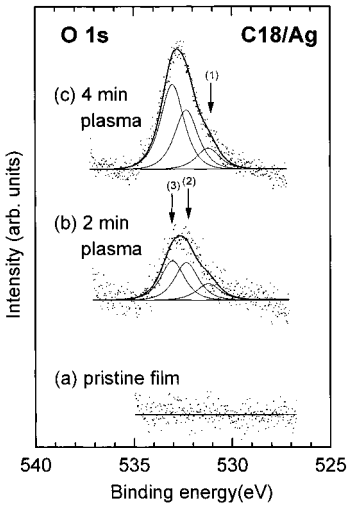

Figure 9. O 1s HRXPS spectra and peak assignments for C18/Ag before (a) and after the plasma treatment for 2 min (b) and 4 min (c). Peak assignment: (1) 531.2 eV − C−O and SO; (2) 532.3 eV − SO_n ($n > 1$); (3) 533.0 eV − N−O.

The observed changes imply above all a decomposition and partial oxidation of the initially intact C18 chains. The downward shift and broadening of the main C 1s peak suggest a partial desorption of hydrogen and cross-linking in the plasma-treated films in the same fashion as it occurs for X-ray or electron irradiation.[6,7,19,22] Note that whereas the BE positions of the C 1s emission for the pristine C18/Au and C18/Ag films were noticeably different (see above), their positions became approximately the same after the plasma treatment. Another general feature is a similar (by ∼20% after 4 min plasma treatment) decrease of the joint C 1s intensity, which is associated with a partial desorption of the carbon-containing fragments or complete C18 chains, again in the same manner as it happens for the X-ray or electron irradiation.[6,7,19,22] Generally, comparing the analogous spectra in Figures 6 and 7, one can conclude that the plasma treatment causes similar changes in the alkyl matrixes of these two films, although the respective processes evolve somewhat slower in the case of C18/Ag.

The situation at the S−substrate interface is essentially different as follows from the S 2p spectra in Figures 4 and 5.

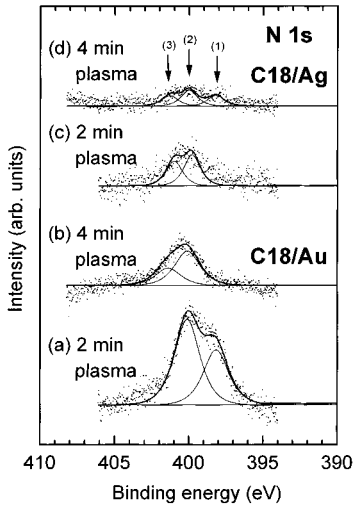

Figure 10. N 1s HRXPS spectra and peak assignments for C18/Au (a,b) and C18/Ag (c,d) after the plasma treatment for 2 min (a,c) and 4 min (b,d). Peak assignment: (1) 398.2 eV, nitride; (2) 400.1 eV, C−N, O−N, and H−N; (3) 401.5 eV, N with C, O-containing species.

Whereas in C18/Au the S 2p doublet related to the pristine thiolate species strongly shrinks after 2 min of the plasma treatment and then disappears completely after 4 min plasma exposure, this doublet remains almost unchanged for a short plasma treatment of C18/Ag (Figure 5b) and decreases its intensity by only 25% after a longer plasma exposure (Figure 5c). Simultaneously, pronounced emissions predominantly related to different sulfones (SO, SO_2, and SO_3) evolve and become dominating in the S 2p spectrum for C18/Au (Figure 5), whereas the intensity of the respective features is significantly smaller than that of the thiolate-related doublet for C18/Ag (Figure 6). This difference is mimicked by the O 1s spectra of the plasma-treated C18 SAMs in Figures 8 and 9, where the peaks related to the oxidized sulfur are much more intense for C18/Au as compared to C18/Ag.

These findings imply an almost complete cleavage of the pristine thiolate−substrate bonds and an extended oxidation of the evolving sulfur species for C18/Au and only a partial cleavage of these bonds and rather moderate extent of the oxidation processes at the sulfur−substrate interface for C18/Ag (the bond cleavage and oxidation occur presumably at the same time). A comparably large entire S 2p intensity (with respect to that for the pristine film) in Figures 4b and 4c is presumably related to the partial desorption of the covering hydrocarbon layer (see below) and a distribution of the plasma-treatment-induced sulfur-containing species over the whole film. The photoelectron signal originated from those species experiences, thus, less attenuation than the corresponding signal from the film−substrate interface and becomes therefore more intense. Basically, oxidized thiolate species are believed to be weakly bound to the substrate.[9,10] However, a definite part of these species can get bound in the alkyl matrix in the same manner as electron-irradiation-induced alkylsulfide moieties.[7]

4. Discussion

The plasma processing of the C18 SAMs on Au and Ag substrates results in massive damage and disordering of the initially well-ordered and chemically homogeneous monomolecular layers. The most noticeable processes are partial desorption of hydrogen and carbon-containing fragments and subsequent cross-linking within the residual layer, partial oxidation of the alkyl matrix, appearance of the nitrogen-containing entities, and cleavage of the sulfur−substrate bonds with simultaneous (presumably) oxidation of the evolving sulfur species. Considering that the majority of the chemical transformations are mediated by oxygen and that the amount of the nitrogen-containing moieties in the plasma-treated C18 films is rather small (as compared to the oxygen-containing moieties), one can conclude that the oxygen-derived constituents in plasma provide the major impact. Assuming that our plasma consists to a greater extent from the nitrogen-derived entities, this finding is a new, very impressive manifestation of the extreme chemical activity of oxygen-derived plasma constituents such as O and O_2 radicals and atomic oxygen.

Comparing the result of the plasma exposure for C18/Au and C18/Ag, we found that whereas the damage of the alkyl matrix in the both films is similar (even if the respective processes are somewhat slower in C18/Ag), the cleavage of the headgroup−substrate bonds and the oxidation processes at the SAM−substrate interface evolve with a smaller rate and to a much lesser extent in C18/Ag than in C18/Au. This behavior implies that the reactions of the alkyl matrix and the S−substrate interface toward plasma processing are only partly correlated and that the S−substrate bond in C18/Ag is noticeably stronger than that in C18/Au. As to the above-mentioned partial correlation, it can be assumed that the pertaining strong anchoring to the substrate after two minutes of the plasma treatment of C18/Ag (Figure 5b) is the reason for a smaller damage of the alkyl matrix in this system (Figure 7b). Alternatively, the almost complete oxidation of the pristine thiolate species at the S−Au interface in C18/Au after even a short plasma exposure (Figure 4b) is accompanied by an extended damage of the aliphatic matrix (Figure 6b). Note that along with the anchoring to the substrate there is another factor, which also affects the rate and extent of the plasma-treatment-related damage in aliphatic matrix of C18/Au and C18/Ag, namely, different packing densities of the alkyl chains, this parameter being larger in the latter system.[1,46−49] However, we assume that the anchoring to the substrate has the major impact, given the relatively small value of this difference and similar damage of the alkyl matrix in C18/Au and C18/Ag.

As to the mentioned difference in the reaction of the S−substrate bond in AT/Au and AT/Ag toward the plasma treatment, similar phenomena were observed at the exposure of AT SAMs on gold and silver substrates by middle-energy (800 eV) He^+ ions,[3] low-energy (10 eV) electrons,[22] and UV-light in the presence of air.[10,11] The same conclusions on an enhanced strength of the S−substrate bond in AT/Ag as compared to AT/Au have been derived.[3,11,22] Additionally, this difference was considered to be the main reason for the dissimilar character of thermal desorption of ethanethiol from Ag(110) and Au(110) surfaces, where sulfur-containing species were released from Au, while an almost complete retention of sulfur could be observed on Ag.[51]

Whereas some of the processes occurring during the exposure of AT SAMs to the nitrogen−oxygen plasma also takes place at the irradiation of these films by X-rays,[4−7] electrons,[13−22] and ions[3] (e.g., partial desorption and cross-linking effects), the entire variety of the changes evoked by the plasma treatment in these systems has the closest resemblance to the damage occurred at UV photooxidation.[8−12] Considering that the damage at the UV exposure in the presence of air is predominately provided by the oxygen-derived reactive species generated by the UV-light, this resemblance supports our conclusion that the atomic oxygen and oxygen radicals provide the major impact in the case of the plasma treatment described in this article.

The appearance of the alkylsulfide species (a BE of S 2p of ~163.2 eV),[7] typical for X-ray- and electron-induced damage,[5−7,18−20,22] and a relatively large downward shift of the C 1s peak (0.5 eV [3] vs ~0.1 eV for C18/Au in this study) do not occur in our case, which agrees with the results of the plasma characterization (Section 3.1) implying a low density and low kinetic energy (most important) of the electrons and ions. At least for electrons, this energy (~0.5 eV) is not sufficient for the dissociative excitation of the individual bonds within the plasma-treated films.[17,21] Thus, the observed modification of the C18 SAMs should be mostly representative for the effect provided by the oxygen radicals.

These radicals seem to be even more reactive than the chemically active oxygen-derived species generated by the UV-light. Whereas an almost complete resemblance between the processes occurring at the S−substrate interface at the UV photooxidation and the plasma exposure can be assumed (based on the similarity of the respective S 2p spectra), a partial oxidation of the alkyl matrix (see Figures 6 and 7) does not take place in the case of the photooxidation.[9,10,12] On the other hand, these oxidation processes can be at least partly related to the appearance of free radicals in the plasma-treated films mediated by a small fraction of "hot" ionizing particles (electrons and ions), which is still present in a low-energy plasma. The amount of these particles is probably not enough to compete with the oxygen radicals at the S−Au interface, but probably adequate to participate to some extent in the oxidation of the alkyl matrix.

On the basis of the results of the UV photooxidation studies, we can assume that the rate-determining step in the photooxidation of C18/Au is the penetration of oxygen radicals to the Au−S interface,[9] while reactivity on Ag is dominated by S−C bond scission. Of course, a higher lateral packing density of the alkyl chains in C18/Ag (as compared to C18/Au) should somewhat slow this penetration in C18 SAM on Ag,[9] however, this small difference (18.4 Å^2 pro AT molecule in AT/Ag vs 21.3 Å^2 in AT/Ag)[1,46−49] cannot fully explain the observed large difference in the extent and rate of the bond-scission and oxidation processes at the S−substrate interface in C18/Au and C18/Ag.

5. Conclusion

Synchrotron-based high-resolution photoelectron spectroscopy was applied to study the modification of the alkanethiol SAMs on gold and silver substrates by nitrogen−oxygen downstream microwave plasma. Although our initial intention was the use of a solely nitrogen plasma, we have not succeeded in avoiding the appearance of the oxygen-containing contaminations in the plasma flow.

The characterization of plasma by a Langmuir probe exhibited a low density and low kinetic energy of the ionizing plasma constituents, such as electrons and ions. It was therefore assumed that the long-lived nitrogen and oxygen radicals provided the major impact of the plasma treatment.

It was found that such a treatment results in massive damage and disordering of the initially well-ordered and chemically homogeneous monomolecular AT layers. The most pronounced processes are the complete (C18/Au) or partial (C18/Ag) oxidation of the pristine thiolate species, partial desorption of hydrogen and carbon-containing fragments with subsequent cross-linking within the residual hydrocarbon layer, and partial oxidation and appearance of the nitrogen-containing entities in this layer. The plasma-treatment-induced processes in the alkyl matrix and at the S−substrate interface are only partly correlated.

The rate and extent of the oxidation processes at the S−substrate interface are noticeably larger for C18/Au as compared to C18/Ag. In particular, almost no thiolate species become damaged or oxidized after a short (2 min) plasma treatment of C18/Ag, whereas the major part of the analogous species in C18/Au was found oxidized after the same plasma exposure. This suggests a stronger S−metal bond in AT/Ag.

The damage of the alkyl matrix in C18/Ag occurs somewhat slower than the respective process in C18/Au, which was explained by the different rate and extent of the oxidation process at the S−substrate interface in C18/Au and C18/Ag and by the difference in the packing density and orientational order of the alkyl matrix in these two systems.

The observation of a large portion of the oxygen-containing moieties in the plasma-treated films and the comparison of the changes caused by the plasma treatment in AT SAMs with the processes occurring at the exposure of these systems to X-rays, electrons, or UV-light (in the presence of air) imply that the major effects are provided by the oxygen radicals, in agreement with the results of the plasma characterization.

The results of this study show that a smallest oxygen contamination should be avoided if one wants to perform a soft modification of thin organic layers or definite molecular entities attached to these layers through a plasma treatment. The future work should include such an option as well as a better control of the plasma composition and parameters of the plasma constituents. Complementary information can be also provided through the variation of the parameters of the plasma-treated organic films. The first experiments on the thioaliphatic SAMs are on the way.

Acknowledgment. We thank the SRRC staff for extensive support during beamtimes, Karin Heister (Universität Heidelberg) for help in the sample preparation, and Prof. T. J. Chuang (National Taiwan University) for providing some experimental equipment for the U5 end stations and two studentships under the *Taiwan Ministry of Education* Grant 89-N-FA01-2-4-5. This work has been supported by the *National Science Council (NSC) of Taiwan* under Grants 89-2320-B-033-005-Y and 89-2112-M-213-016, by the *German Bundesministerium für Bildung und Forschung* through Grants 05 SF8VHA 1, and by the DAAD-NSC exchange program under the PPP Grant 10.

References and Notes

(1) Ulman, A. *An Introduction to Ultrathin Organic Films: Langmuir−Blodgett to Self-Assembly*; Academic Press: New York, 1991; *Chem. Rev.* **1996**, *96*, 1533.

(2) *Thin films: self-assembled monolayers of thiols*; Ulman A., Ed.; Academic Press: San Diego, CA, 1998.

(3) Chenakin, S. P.; Heinz, B.; Morgner, H. *Surf. Sci.* **1999**, *421*, 337.

(4) Laibinis, P. E.; Graham, R. L.; Biebuyck, H. A.; Whitesides, G. M. *Science* **1991**, *254*, 981.

(5) Jäger, B.; Schürmann, H.; Müller, H. U.; Himmel, H. J.; Neumann, M.; Grunze, M.; Wöll, Ch. *Z. Phys. Chem.* **1997**, *202*, 263.

(6) Wirde, M.; Gelius, U.; Dunbar, T.; Allara, D. L. *Nucl. Instrum. Methods Phys. Res. B* **1997**, *131*, 245.

(7) Heister, K.; Zharnikov, M.; Grunze, M.; Johannson, L. S. O.; Ulman, A. *Langmuir* **2001**, *17*, 8.

(8) Lewis, M.; Tarlov, M. J.; Carron, K. *J. Am. Chem. Soc.* **1995**, *117*, 9574.

(9) Hutt, D. A.; Leggett, G. J. *J. Phys. Chem. B* **1996**, *100*, 6657.

(10) Hutt, D. A.; Cooper, E.; Leggett, G. J. *J. Phys. Chem. B* **1998**, *102*, 174.

(11) Cooper, E.; Leggett, G. J. *Langmuir* **1998**, *14*, 4795.

(12) Riely, H.; Kendall, G. K.; Zemicael, F. W.; Smith, T. L.; Yang, S. *Langmuir* **1998**, *14*, 5147.

(13) Baer, D. R.; Engelhard, M. H.; Schulte, D. W.; Guenther, D. E.; Wang, L.-Q.; Rieke, P. C. *J. Vac. Sci.* **1994**, *A12*, 2478.

(14) Rowntree, P.; Dugal, P. C.; Hunting, D.; Sanche, L. *J. Phys. Chem.* **1996**, *100*, 4546.

(15) Seshadri, K.; Froyd, K.; Parikh, A. N.; Allara, D. L.; Lercel, M. J.; Craighead, H. G. *J. Phys. Chem*. **1996**, *100*, 15900.
(16) Müller, H. U.; Zharnikov, M.; Völkel, B.; Schertel, A.; Harder, P.; Grunze, M. *J. Phys. Chem. B* **1998**, *102*, 7949.
(17) Olsen, C.; Rowntree, P. A. *J. Chem. Phys.* **1998**, *108*, 3750.
(18) Zerulla, D.; Chasse, T. *Langmuir* **1999**, *15*, 5285.
(19) Zharnikov, M.; Frey, S.; Gölzhäuser, A.; Geyer, A.; Grunze, M. *Phys. Chem. Chem. Phys*. **1999**, *1*, 3163.
(20) Heister, K.; Frey, S.; Gölzhäuser, A.; Ulman, A.; Zharnikov, M. *J. Phys. Chem. B* **1999**, *103*, 11098.
(21) Huels, M. A.; Dugal, P. C.; Sanche, L. To be published.
(22) Zharnikov, M.; Frey, S.; Heister, K.; Grunze, M. *Langmuir* **2000**, *16*, 2697.
(23) Geyer, W.; Stadler, V.; Eck, W.; Zharnikov, M.; Gölzhäuser, A.; Grunze, M. *Appl. Phys. Lett.* **1999**, *75*, 2401.
(24) Maoz, R.; Cohen, S. R.; Sagiv, J. *Adv. Mater*. **1999**, *11*, 55.
(25) Eck, W.; Stadler, V.; Geyer, W.; Zharnikov, M.; Gölzhäuser, A.; Grunze, M. *Adv. Mater*. **2000**, *12*, 805.
(26) Tiberio, R. C.; Craighead, H. G.; Lercel, M. J.; Lau, T.; Sheen, C. W.; Allara, D. L. *Appl. Phys. Lett.* **1993**, *62*, 476.
(27) Lercel, M. J.; Tiberio, R. C.; Chapman, P. F.; Craighead, H. G.; Sheen, C. W.; Parikh, A. N.; Allara, D. L. *J. Vac. Sci. Technol. B* **1993**, *11*, 2823.
(28) Lercel, M. J.; Redinbo, G. F.; Pardo, F. D.; Rooks, M.; Tiberio, R. C.; Simpson, P.; Craighead, H. G.; Sheen, C. W.; Parikh, A. N.; Allara, D. L. *J. Vac. Sci. Technol. B* **1994**, *12*, 3663.
(29) Lercel, M. J.; Redinbo, G. F.; Rooks, M.; Tiberio, R. C.; Craighead, H. G.; Sheen, C. W.; Allara, D. L. *Mircroelectron. Eng.* **1995**, *27*, 43.
(30) Lercel, M. J.; Rooks, M.; Tiberio, R. C.; Craighead, H. G.; Sheen, C. W.; Parikh, A. N.; Allara, D. L. *J. Vac. Sci. Technol. B* **1995**, *13*, 1139.
(31) Müller, H. U.; David, C.; Völkel, B.; Grunze, M. *J. Vac. Sci. Technol. B* **1995**, *13*, 2846.
(32) David, C.; Müller, H. U.; Völkel, B. Grunze, M.; *Microelectron. Eng.* **1996**, *30*, 57.
(33) Lercel, M. J.; Craighead, H. G.; Parikh, A. N.; Seshadri, K.; Allara, D. L. *J. Vac. Sci. Technol. A* **1996**, *14*, 1844.
(34) Hild, R.; David, C.; Müller, H. U.; Völkel, B.; Kayser, D. R.; Grunze, M. *Langmuir* **1998**, *14*, 342.
(35) Sugimura, H.; Ushiyama, K.; Hozumi, A.; Takai, O. *Langmuir* **2000**, *16*, 885.
(36) Gölzhäuser, A.; Geyer, W.; Stadler, V.; Eck, W.; Grunze, M.; Edinger, K.; Weimann, Th.; Hinze, P. *J. Vac. Sci. Technol. B* **2000**, *18*, 3414.
(37) Unger, W. E. S.; Lippitz, A.; Gross, Th.; Friedrich, J. F.; Wöll, Ch.; Nick, L. *Langmuir* **1999**, *15*, 1161.
(38) Liao, J.-D.; Rieu, J.; Demuth, O.; Corre, Y. *Biomed. Eng.: Appl., Basis, Comm.* **1994**, *6*, 49.
(39) *Handbook of Ion Sources*; Wolf, B. H., Ed.; CRC Press: Boca Raton, FL, 1995; Chapter 2.
(40) Liao, J.-D.; Wu, T.-H.; Tseng, T.-L. *Proc. Soc. Mater. Sci.* **1997**, *1*, 13.
(41) Chen, Y.-W.; Liao, J.-D.; Kau, J.-Y.; Huang, J.; Chang, W.-T. *Marcomolecules* **2000**, *33*, 5638.
(42) Grill, A. *Cold Plasma in Materials Fabrication: from fundamentals to applications*; IEEE Press: 1993; pp 129-137.
(43) Spanel, P. *J. Mass Spectrom. Ion Processes* **1995**, *149*−*150*, 299.
(44) Liao, J.-D.; Yu, Y.-S.; Wei, P. *Chung Yuan J.* **1999**, *27*−*1*, 89.
(45) Tyan, Y.-C.; Liao, J.-D.; Klauser, R.; Wu, I.-D.; Weng, C.-C. *Biomaterials*, in press.
(46) Laibinis, P. E.; Whitesides, G. M.; Allara, D. L.; Tao, Y.-T.; Parikh, A. N.; Nuzzo, R. G. *J. Am. Chem. Soc.* **1991**, *113*, 7152.
(47) Fenter, P.; Eisenberger, P.; Liang, K. S. *Phys. Rev. Lett.* **1993**, *70*, 2447; Fenter, P.; Eberhardt, A.; Eisenberger, P. *Science* **1994**, *266*, 1216.
(48) Camillone, N., III; Chidsey, C. E. D.; Liu, G.; Scoles, G. *J. Chem. Phys.* **1993**, *98*, 3503; *J. Chem. Phys.* **1993**, *98*, 4234.
(49) Poirier, G. E.; Tarlov, M. J. *Langmuir* **1994**, *10*, 2853.
(50) Walczak, M. M.; Chung, C.; Stole, S. M.; Widrig, C. A.; Porter, M. D. *J. Am. Chem. Soc.* **1991**, *113*, 2370.
(51) Jaffey, D. M.; Madix, R. J. *Surf. Sci.* **1994**, *311*, 159.
(52) Lestelius, M.; Liedberg, B.; Tengvall, P. *Langmuir* **1997**, *13*, 5900.
(53) Feldman, K.; Hähner, G.; Spendcer, N. D.; Harder, P.; Grunze, M. *J. Am. Chem. Soc.* **1999**, *121*, 10134.
(54) Köhn, F. Diploma Thesis, Universität Heidelberg, Heidelberg, Germany, 1998.
(55) Heister, K.; Zharnikov, M.; Grunze, M.; Johansson, L. S. O. *J. Phys. Chem. B* **2001**, *105*, 4058.
(56) Moulder, J. F.; Stickle, W. E.; Sobol, P. E.; Bomben, K. D. *Handbook of X-ray Photoelectron Spectroscopy*; Chastian, J., Ed.; Perkin-Elmer Corp.: Eden Prairie, MN, 1992.
(57) Welle, A.; Liao, J.-D.; Kaiser, K.; Grunze, M.; Mader, U.; Blank, N. *Appl. Surf. Sci.* **1997**, *119*, 185.
(58) Liao, J. D. *Macromolecules*, in press.
(59) Himmelhaus, M.; Gauss, I.; Buck, M.; Eisert, F.; Wöll, Ch.; Grunze, M. *J. El. Spectrosc. Relat. Phenom.* **1998**, *92*, 139.
(60) Siegbahn, K.; Nordling, C.; Fahlman, A.; Nordberg, R.; Hamrin, K.; Hedman, J.; Johansson, G.; Bergmark, T.; Karlsson, S.-E.; Lindgren, I.; Lindberg, B. *Nova acta regiae societatis scientiarum upsaliensis* **1967**, *IV*, 118.
(61) Lee, M.-T.; Hsueh, C.-C.; Freund, M. S.; Ferguson, G. S. *Langmuir* **1998**, *14*, 6419.